Micropipet-Based Pico Force Transducer: In Depth Analysis and Experimental Verification

D. A. Simson, F. Ziemann, M. Strigl, and R. Merkel
Lehrstuhl für Biophysik, Technische Universität München, D-85748 Garching, Germany

ABSTRACT Measurements of forces in the piconewton range are very important for the study of molecular adhesion and mechanics. Recently, a micropipet-based force transducer for this type of experiment was presented (E. Evans, K. Ritchie, and R. Merkel, 1995, *Biophys. J.*, 68:2580–2587). In the present article we give a detailed mechanical analysis of this transducer, including nonlinear effects. An analytical expression for the transducer stiffness at small elongations is given. Using magnetic tweezers (F. Ziemann, J. Rädler, and E. Sackmann, 1994, *Biophys. J.*, 66:2210–2216), we were able to determine the force displacement relation of this transducer experimentally. Forces from approximately 10 pN to 500 pN were applied. Theoretical predictions and experimental results coincide remarkably well.

INTRODUCTION

Many processes in biological systems involve forces between single molecules. Prominent examples are motor proteins (Simmons, 1996), transcription of DNA, and cell adhesion (Bongrand et al., 1994). In all cases the relevant forces range from 1 pN to some 100 pN. Measurement of such minuscule forces is a difficult task, and many different experimental techniques have been applied. Atomic force microscopy is the best established technique to date (Florin et al., 1994; Dammer et al., 1996; Lee et al., 1994). Forces from approximately 10 pN to several nanonewtons can be measured. Combination with light microscopic techniques is possible but very difficult. Another approach is the bending of glass micro-needles (Kishino and Yanagida, 1988). In both techniques, soft springs are used, the stiffness of which cannot be changed during the experiment. This problem has been overcome by the following techniques that allow simple tuning of the force range. Application of hydrodynamic forces (Pierres et al., 1995; Tees and Goldsmith, 1996; Kuo and Lauffenburger, 1993; Alon et al., 1995) allows tuning of the acting force via the flow rate. Forces from 1 pN upwards can be applied. Unfortunately, the evaluation of the data is very difficult, and only very specific geometries can be used. Using optical tweezers is another very elegant technique (Ashkin et al., 1990; Svoboda et al., 1993; Finer et al., 1994). Optical tweezers allow tuning of the trap stiffness, and the combination with high-resolution light microscopy is part of the technique. This makes the technique well suited for experiments on cells (Hochmuth et al., 1996). Nevertheless, due to the occurrence of radiation damage, only forces below approximately 50 pN can be applied. In recent years micropipet techniques have been developed that overcome the above mentioned problems at least partially (Evans et al., 1991, 1995; Shao and Hochmuth, 1996; Chesla and Zhu, 1996).

In this paper, we present an in-depth analysis of a micromechanical force transducer that was developed by Evans and co-workers (Evans et al., 1995; Yeung, 1994) and an experimental verification of this analysis. The force transducer is shown in Fig. 1. It consists of an osmotically preswollen human red blood cell that is aspirated into a micropipet. Exactly opposite to the entrance of the pipet a microbead is glued onto the red blood cell. Membrane tension opposes deflection of the microbead. The main advantage of this force transducer is that by simply changing the suction pressure of the micropipet its stiffness can be tuned from 0.04 m/m to some millinewtons per meter during experiments. Thus, it is a highly flexible tool for the measurement of the smallest forces. The design of the transducer is aimed at preserving axial symmetric geometry even with forces acting. This symmetry greatly simplifies the theoretical analysis. The microbead serves a twofold purpose. First, it distributes a mechanical point load over a large area and thus prevents formation of membrane tethers and contributions of membrane bending moments to the force (Evans et al., 1991). Therefore, cell-specific parameters (i.e., bending and in-plane shear module) do not influence the transducer stiffness. A second important point is the availability of microbeads with different surface properties and the possibility of covalent linkage of biologically relevant molecules (proteins and DNA) to the bead surface.

Forces are measured via the displacement of the microbead. Therefore, the detailed knowledge of the force displacement relation is a necessary prerequisite for the application of any force transducer. We calculated the force displacement relation, including all nonlinear effects. For small elongations an analytical expression for the transducer stiffness is given. Several assumptions enter the theoretical analysis. Namely, preservation of axial symmetry and neglection of all in-plane shear and membrane-bending effects. Therefore, it is necessary to verify this analysis by an experimental approach. We used paramagnetic microbeads

Received for publication 26 August 1997 and in final form 5 January 1998.
Address reprint requests to Dr. R. Merkel, Physics Department, Technical University Munich, Biophysics Group E22, James-Frank-Strasse 1, D-85748 Garching, Germany. Tel.: 49-89-2891-2480; Fax: 49-89-2891-2469; E-mail: rmerkel@physik.tu-muenchen.de.
© 1998 by the Biophysical Society
0006-3495/98/04/2080/09 $2.00

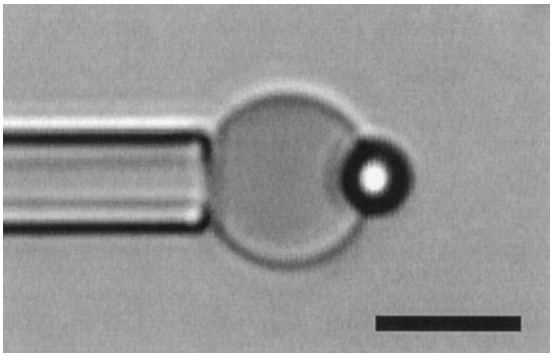

FIGURE 1 Micrograph of the force transducer. Scale bar, 5 μm.

(Dynabeads) and applied calibrated magnetic forces. This technique is known as magnetic tweezers and allows application of very low forces with high accuracy (Ziemann et al., 1994; Heinrich and Waugh, 1996). Magnetic forces ranged from approximately 10 pN to 500 pN. With light microscopy and digital image processing we were able to determine the bead position with an error of at most 5 nm. Thus we could determine the force displacement relation experimentally. The experimental results coincided with the calculated curves. This proves that highly accurate force measurements are possible with this specific type of force transducer. Forces ranging from 0.25 pN to several nanonewtons can be measured.

MECHANICAL ANALYSIS

Assumptions and description

A mechanical analysis of the force transducer will be presented here. The whole assembly of the force transducer is axially symmetric. The symmetry axis is the center line of the pipet. External forces act on the bead exclusively along the axis of symmetry. In our case, a calibrated magnetic force is applied. Generally, the force might be due to mechanical probing of a cell membrane or of specific receptor ligand bonds. With an external force applied along the axis of symmetry, the shape of the membrane is no longer spherical. Nevertheless, axial symmetry is preserved because osmotic preswelling of the red blood cell prevents formation of dimples or folds. The main purpose of this analysis is the determination of the force extension relation of the force transducer. The analysis is simplified by the mechanical properties of the erythrocyte membrane. Its membrane area elastic modulus was found to be 450 mN/m (Evans et al., 1976; Evans and Waugh, 1977), whereas the elastic modulus for in-plane shear is on the order of 10 μN/m (Evans, 1973; Hochmuth et al., 1973). Compared with the above mentioned deformation modes, bending rigidity is usually negligible (Evans and Skalak, 1980; Evans and Rawicz, 1990; Zilker et al., 1992). In our experiments, we always worked in a range of membrane tensions where shear and bending elasticity could be safely neglected. In fact, we found that we had to work in this regime to aspirate a preswollen red blood cell properly into the pipet. Therefore, in-plane shear and bending effects will be ignored in the following analysis. Membrane surface area and enclosed volume are assumed to be preserved. The justification for this assumption will be presented later. Area and volume conservation will be used to determine the geometrical parameters of the deformed cell.

The membrane of the force transducer can be neatly divided into four distinct regions (see Fig. 2). The aspirated part consists of a cylindrical part where the suction pressure of the pipet forces the membrane against the pipet wall and of a hemispherical cap. This cap is hemispherical only as long as the membrane tension exceeds the in-plane shear module (Evans, 1973). The part of the membrane that is adhered to the microbead is assumed to be completely fixed. The middle part of the membrane is free. Its form is governed by the interplay of hydrostatic pressure and membrane tension. As shear stress can be neglected, membrane tension is constant over the free part of the membrane. The hydrostatic pressure is also constant over the whole surface. Therefore it follows from the law of Young and Laplace that the free part of the membrane must be a surface of constant mean curvature (Evans and Skalak, 1980). It is the form of this free membrane that we will deal with mostly in the remainder of the analysis.

Please note that alternative approaches to the problem are possible (for an example see Zhu et al., 1994). These authors also obtained an expression for the form of the free part of the membrane and applied it to the problem of cell-cell adhesion.

Calculation of the force elongation relation

It is important to realize that the mechanical properties of the force transducer are entirely determined by the shape of the free part of the membrane. Therefore we will give an explicit formula for the geometrical form and develop a technique for the determination of all free parameters.

The mean curvature $\bar{c}$ is determined by the acting external force f and the suction pressure of the pipet ΔP. The law of Young and Laplace is

$$\bar{c} = \frac{P_i - P_o}{\tau}, \tag{1}$$

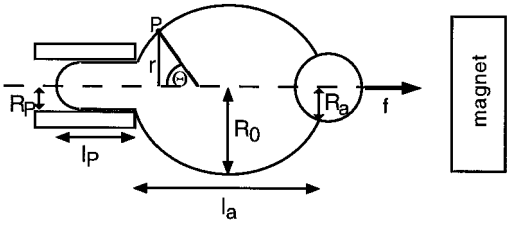

FIGURE 2 The geometry of the transducer. In the lower half the physical dimensions are defined, and in the upper half are the coordinates of the point P. The dashed line is the axis of symmetry. Definitions of the symbols are given in the text.

where P_i denotes the hydrostatic pressure inside the red blood cell, P_o in the sample chamber, and τ is the membrane tension. The mean curvature is defined by $\bar{c} = 1/R_1 + 1/R_2$ where R_1 and R_2 denote the two principle radii of curvature. The membrane slides freely along the walls of the pipet (Evans, 1973; Discher and Mohandas, 1996); therefore, membrane tension τ is continuous at the pipet entrance. Free body diagrams of the erythrocyte cut at the mouth of the pipet (see Fig. 3) yield the following equilibrium conditions (Yeung, 1994):

$$\pi R_p^2(P_i - P_p) = 2\pi R_p \tau \tag{2}$$

$$\pi R_p^2(P_i - P_o) + f = 2\pi R_p \tau \sin\theta_p, \tag{3}$$

where R_p denotes the inner radius of the pipet, P_p the pressure inside the pipet, f the acting external force, and θ_p the angle of the membrane normal directly at the entrance of the pipet to the axis of symmetry (see Fig. 3). Basic algebra yields the membrane tension

$$\tau = \frac{\Delta P R_p}{2(1 - \sin\theta_p)}(1 - \hat{f}). \tag{4}$$

Here $\hat{f}$ is the normalized force defined by

$$\hat{f} = f/(\Delta P \pi R_p^2), \tag{5}$$

and ΔP equals $(P_o - P_p)$. Equations 1, 3, and 4 combined yield a relation between the acting force and the mean curvature of the free part of the transducer membrane:

$$\hat{f} = \frac{\bar{c} - 2\sin\theta_p/R_p}{\bar{c} - 2/R_p}. \tag{6}$$

The axisymmetric shape of the free membrane is best parameterized by the coordinates r and θ, where r is the distance from the axis of revolution and θ the angle between the surface normal and the axis of revolution (see Fig. 2). In this coordinate system the mean curvature $\bar{c}$ is given by (Evans and Skalak, 1980)

$$\bar{c} = \frac{\sin\theta}{r} + \frac{d(\sin\theta)}{dr}. \tag{7}$$

As the free part of the membrane is a form of constant mean curvature, Eq. 7 can be easily integrated. It is found that any form of constant mean curvature with an intermediate extremum of the radius (an apex) is described by Evans, 1980:

$$\sin\theta = \begin{cases} \dfrac{1}{r}\dfrac{(R_0 - R_p\sin\theta_p)r^2 + R_pR_0(R_0\sin\theta_p - R_p)}{R_0^2 - R_p^2}, \\ \qquad\qquad \text{left of the apex} \\ \dfrac{1}{r}\dfrac{(R_0 - R_a\sin\theta_a)r^2 + R_aR_0(R_0\sin\theta_a - R_a)}{R_0^2 - R_a^2}, \\ \qquad\qquad \text{right of the apex} \end{cases} \tag{8}$$

This equation has five parameters, namely, the pipet radius R_p, the pipet angle θ_p, the radius of the adhesion disk R_a, the angle of the membrane normal to the axis of revolution at the contact of the membrane to the microbead θ_a, and the maximal radius assumed by the form R_0 (see also Fig. 2). As the mean curvature $\bar{c}$ must be the same on both sides of the apex, the following relation between the five parameters exists:

$$\bar{c} = 2\frac{R_0 - R_p\sin\theta_p}{R_0^2 - R_p^2} = 2\frac{R_0 - R_a\sin\theta_a}{R_0^2 - R_a^2}. \tag{9}$$

Later this relation will be used to eliminate θ_a. Of the remaining four parameters, the pipet radius R_p and the radius of the adhesion disk R_a are given by the geometry of the experiment. The remaining two parameters, R_0 and θ_p, are adjustable and have to be found by the constraints of area and volume conservation.

Membrane surface and enclosed volume are given by

$$A = 2\pi R_p l_p + \int_0^{l_a} 2\pi r\sqrt{1 + (dr/dz)^2}\,dz \tag{10}$$

$$V = \pi R_p^2(l_p - R_p) + 2\pi R_p^3/3 + \int_0^{l_a} \pi r^2\,dz. \tag{11}$$

Here, l_p denotes the projection length. The terms describing the adhered part of the membrane were dropped as the geometry is fixed there. Please note that the projection length is an additional adjustable parameter. The extension l_a is given by

$$l_a = \int_0^{l_a} dz. \tag{12}$$

In these integrals the form is parameterized in standard polar coordinates and axial symmetry is assumed. To use Eq. 8 for the form we must first transform the coordinates.

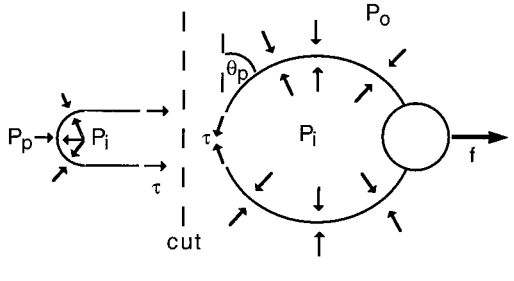

FIGURE 3 Free body diagram of the transducer. In mechanical equilibrium the sum of all internal and external forces acting on any part of a body must vanish. Here we consider the erythrocyte cut at the mouth of the pipet by an imaginary plane perpendicular to the axis of symmetry. In this case the external forces are the pressures acting across the membrane and the magnetic force f acting on the bead. Surface tension τ is the only internal force field. The surface tension must balance the integrated external forces. Only force components parallel to the axis of symmetry were considered. The left diagram yields Eq. 2, the right one Eq. 3.

In the following we will show how to deal with Eq. 10. The other integrals can be handled in a completely analogous way.

From differential geometry, the following equation holds (Evans and Skalak, 1980):

$$\left|\frac{dz}{dr}\right| = \tan\theta. \tag{13}$$

It can be applied to perform the necessary transformation of the coordinates.

$$\int_0^{l_a} 2\pi r\sqrt{1+(dr/dz)^2}dz = \int_{R_p}^{R_0} 2\pi r \frac{1}{\sqrt{1-\sin^2\theta}}dr + \int_{R_a}^{R_0} 2\pi r \frac{1}{\sqrt{1-\sin^2\theta}}dr. \tag{14}$$

Now we are able to use Eq. 8 for $\sin\theta$. Equation 14 can be integrated with the help of elliptical integrals. Instead of this approach we used a series expansion technique that allowed straightforward derivation of the stiffness at small applied force. First, we assume that the shape of the free membrane part is close to a sphere and introduce parameters ϵ_a and ϵ_p that describe the deviation from the spherical form and are therefore small quantities:

$$\epsilon_a = \sin\theta_a - R_a/R_0; \quad \epsilon_p = \sin\theta_p - R_p/R_0. \tag{15}$$

If we insert these definitions in Eq. 8, we get the following result for the shape of the free membrane:

$$\sin\theta = (1-\alpha)\rho + \alpha/\rho, \tag{16}$$

where the abbreviations $\rho = r/R_0$ and

$$\alpha = \frac{R_0R_a\epsilon_a}{R_0^2-R_a^2} = \frac{R_0R_p\epsilon_p}{R_0^2-R_p^2} \tag{17}$$

have been used. For the last identity we used Eq. 9. The parameter α has a simple geometrical meaning. It describes the relative deviation of the deformed transducer's mean curvature from that of a sphere with equal radius R_0. Please note that α is a small parameter as well. Now we expand the troublesome integrand in Eq. 14 with respect to α.

$$\frac{\rho}{\sqrt{1-\sin^2\theta}} = \frac{1}{\sqrt{1-\rho^2}}\sum_{n=0}^{\infty}\binom{-1/2}{n}(\alpha^2-2\alpha)^n \sum_{l=0}^{n}\binom{n}{l}\left(\frac{\alpha}{2-\alpha}\right)^l \rho^{-2l+1} \tag{18}$$

In this form all terms in the sum can be integrated analytically (Gröbner and Hofreiter, 1975):

$$I_N(\rho) = \int_\rho^1 \frac{1}{x^N\sqrt{1-x^2}}dx$$

$$I_N(\rho) = \begin{cases} \rho^2/3\sqrt{1-\rho^2} + 2/3\sqrt{1-\rho^2} & : \quad N=-3 \\ \sqrt{1-\rho^2} & : \quad N=-1 \\ \ln\left(\dfrac{\rho}{1-\sqrt{1-\rho^2}}\right) & : \quad N=1 \end{cases}$$

$$I_{N+2}(\rho) = \frac{\sqrt{1-\rho^2}}{(N+1)\rho^{N+1}} + \frac{NI_N(\rho)}{N+1} : \ \forall N = 1, 3, 5, \ldots \tag{19}$$

Collecting all terms we get

$$A = 2\pi R_p l_p + 2\pi R_0^2 \Xi_A(\epsilon_p, R_0)$$

$$\Xi_A(\epsilon_p, R_0) = G_A(\alpha, \rho_a) + G_A(\alpha, \rho_p)$$

$$G_A(\alpha, \rho) = \sum_{n=0}^{\infty}\binom{-1/2}{n}(\alpha^2-2\alpha)^n \times \sum_{l=0}^{n}\binom{n}{l}\left(\frac{\alpha}{2-\alpha}\right)^l I_{2l-1}(\rho), \tag{20}$$

where ρ_a is defined as $\rho_a = R_a/R_0$ and $\rho_p = R_p/R_0$, respectively. The expressions for the enclosed volume, Eq. 11, and for the extension of the transducer, Eq. 12, were treated in the same way. The resulting expressions are

$$V = \pi R_p^2(l_p - R_p) + 2\pi R_p^3/3 + \pi R_0^3 \Xi_V(\epsilon_p, R_0)$$

$$\Xi_V(\epsilon_p, R_0) = G_V(\alpha, \rho_a) + G_V(\alpha, \rho_p)$$

$$G_V(\alpha, \rho) = \sum_{n=0}^{\infty}\binom{-1/2}{n}(\alpha^2-2\alpha)^n \times \sum_{l=0}^{n}\binom{n}{l}\left(\frac{\alpha}{2-\alpha}\right)^l ((1-\alpha)I_{2l-3}(\rho) + \alpha I_{2l-1}(\rho)). \tag{21}$$

$$l_a = R_0 \Xi_z(\epsilon_p, R_0)$$

$$\Xi_z(\epsilon_p, R_0) = G_z(\alpha, \rho_a) + G_z(\alpha, \rho_p)$$

$$G_z(\alpha, \rho) = \sum_{n=0}^{\infty}\binom{-1/2}{n}(\alpha^2-2\alpha)^n \times \sum_{l=0}^{n}\binom{n}{l}\left(\frac{\alpha}{2-\alpha}\right)^l ((1-\alpha)I_{2l-1}(\rho) + \alpha I_{2l+1}(\rho)). \tag{22}$$

The terms of the series are proportional to $(\epsilon_a/(1-(R_a/R_0)^2))^{2n}$. Therefore, the series in Eqs. 20–22 converge very fast for all practical situations. To determine the initial conditions, surface area, enclosed volume, and extension are calculated with the experimentally determined parameters in the force-free state: radius of the spherical part $R_{0,0}$ and projection length $l_{p,0}$. Moreover, α and ϵ are zero in the force-free state; therefore, Eqs. 20–22 yield closed analytical expressions in this case. The expressions for surface area and enclosed volume contain three adjustable parameters: l_p, ϵ_p, and R_0. Two conditions, area and volume con-

servation, must be satisfied. Thus, we are able to determine two of the free parameters uniquely as a function of the third for any initial condition (e.g., for any given area and volume). In other words, we are now able to calculate the extension l_a for all values of the mean curvature $\bar{c}$. As the mean curvature yields directly the force (see Eq. 6), the complete force extension relation can be calculated for any given initial conditions.

As the functions involved are highly nontrivial, numerical computation seems to be the only way to deal with the problem. The projection length can be eliminated from the two conditions for area and volume conservation. The numerical problem is now reduced to root finding of a one-dimensional function.

$$F(\epsilon_p, R_0(\epsilon_p)) = 0$$

$$\begin{aligned} F(\epsilon_p, R_0) = {} & R_p R_{0,0}^2 \Xi_A(\epsilon_p = 0, R_{0,0}) \\ & - R_p R_0^2 \Xi_A(\epsilon_p, R_0) - R_{0,0}^3 \Xi_V(\epsilon_p = 0, R_{0,0}) \\ & + R_0^3 \Xi_V(\epsilon_p, R_0). \end{aligned} \tag{23}$$

Values for ϵ_p were given, and the resulting function $R_0(\epsilon_p)$ was determined using Brent's algorithm (Stoer and Bulirsch, 1993). Please remember that ϵ_p describes the deviation of the shape from a sphere. With this relation, we finally determined the shape of the free part of the membrane for any given ϵ_p (see Eqs. 8 and 15). Equation 9 allows the determination of the mean curvature and together with Eq. 6 the acting force. The extension of the transducer for this specific value of ϵ_p can be calculated using Eq. 22. Thus, we are able to determine the desired force extension relation. An example is presented in Fig. 4. As can be seen, nonlinear effects cannot be neglected for extensions of more than approximately 200 nm.

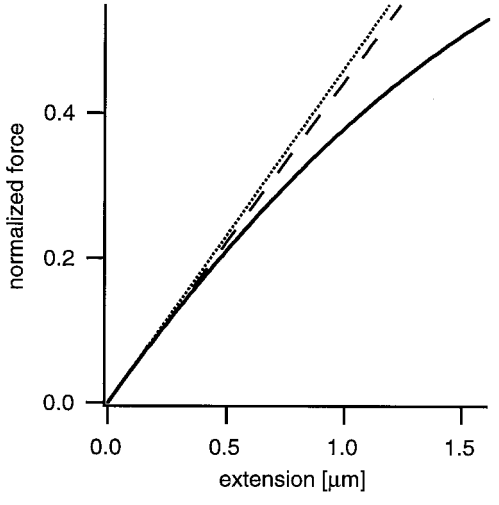

FIGURE 4 Force extension relation calculated for $R_{0,0} = 3$ μm, $R_P = 1$ μm, and $R_a = 0.5$ μm. The solid curve shows the numerical solution (Eq. 23), the dotted line shows the first-order expansion (Eq. 25), and the dashed line shows the approximate first-order expansion (Eq. 26).

At this point it is a simple task to introduce area elasticity and pressure-induced volume changes in the calculation. We added the corresponding terms to Eqs. 20–22 and modified Eq. 23 accordingly. The area elastic modulus and the osmotic activity were taken from (Evans and Waugh, 1977). For membrane tensions up to 10 mN/m, force extension relations calculated assuming varying volume and surface area could not be distinguished from the results for fixed area and volume. The maximal relative deviations of force, membrane tension, and hydrostatic pressure were less than 2×10^{-4} and less than 10^{-3} for the extension. Forces up to 19 nN were used for this calculation. As 10 mN/m is the lysis tension of human red blood cells (Evans et al., 1976), the assumptions of fixed volume and surface area hold for all practical purposes.

Stiffness for small extensions

The force extension relation is linear for small extensions below 200–300 nm. In this regime, the shape of the free part of the membrane is very close to a sphere. Therefore, α is very small and we can develop all parameters to first order in α. Nevertheless, area and volume must be conserved and we have to satisfy Eq. 23 to first order in α. This yields a variation of the maximal radius of the free part of the membrane, R_0, with the extension. We find

$$R_0 = R_{0,0} - \beta\alpha + \mathcal{O}(\alpha^2)$$

$$\beta = R_{0,0} \frac{(1-\rho_p)(\sqrt{1-\rho_p^2} + \sqrt{1-\rho_a^2})}{A\sqrt{1-\rho_p^2} + B\sqrt{1-\rho_a^2} + C/\sqrt{1-\rho_a^2} + D/\sqrt{1-\rho_p^2}}$$

$$A = 2 + \rho_p^2/3 - 2\rho_p$$

$$B = 2 + \rho_a^2/3 - 2\rho_p$$

$$C = 2\rho_a^2/3 - \rho_a^2\rho_p + \rho_a^4/3$$

$$D = 2\rho_p^2/3 - \rho_p^3 + \rho_p^4/3. \tag{24}$$

Expansion of Eqs. 6, 22, and 7 to first order in α yields the transducer stiffness k at small extensions:

$$k = \lim_{f \to 0} \frac{f}{l_a(f) - l_a(f=0)}$$

$$k = \frac{\pi R_p^2 \Delta P}{(\rho_p - \rho_p^2)(R_{0,0} I_1(\rho_a) + R_{0,0} I_1(\rho_p) - \beta E)}$$

$$E = \sqrt{1-\rho_p^2} + \sqrt{1-\rho_a^2} + \frac{\rho_a^2}{\sqrt{1-\rho_a^2}} + \frac{\rho_p^2}{\sqrt{1-\rho_p^2}}. \tag{25}$$

Fortunately, in most practical cases, ρ_a and ρ_p are small quantities and the above equation can be expanded. Includ-

ing second-order terms we get

$$k = \frac{R_p \Delta P}{2(1-\rho_p)} \frac{2\pi}{\ln\left(\frac{4}{\rho_a \rho_p}\right) - (1 - \rho_p/4 - 3\rho_p^2/8 + \rho_a^2)}. \quad (26)$$

In most circumstances, this approximation is sufficient as long as the extensions remain below 200–300 nm. The relative deviation between Eqs. 25 and 26 is approximately 5%. For larger extensions, nonlinear effects play a role and the full numerical calculation should be used.

MATERIALS AND METHODS

Micromanipulation

A general description of a micropipet setup can be found in Needham, 1993. Micropipets were pulled from borosilicate glass capillaries (Hilgenberg, Malsfeld, Germany) using a Flaming Brown micropipet puller (P-87, Sutter Instruments, San Rafael, CA) and broken by insertion in a molten drop of soda lime glass, cooling the glass and shearing the pipet off the drop. Breaking was done with the help of a dissecting microscope (Carl Zeiss, Jena, Germany). The broken pipets had an inner diameter of 1.3–2.0 μm, which did not change noticeably over at least 100 μm. The inner diameter was determined accurately by insertion of calibrated glass microneedles as described by Evans, 1989. These needles were pulled into a cone shape with an opening angle of approximately 2.5° and gold sputtered. The exact shape was determined by scanning electron microscopy. Needles were inserted as far as possible into the pipet, and the insertion length was measured using the light microscope. The diameter of the glass microneedle at this distance from the tip was taken from the scanning electron microscopy micrographs and represented the inner diameter of the pipet. Diameters could be determined with an error of at most 100 nm. The broken pipets were filled with buffer and inserted in a micromanipulator (MMN-1, Narishige International, London, UK). Pressure differences between the chamber and the pipet were applied as described in Needham, 1993, and measured with a differential pressure transducer (DP15-26, Validyne, Northridge, CA). Micromanipulation was done in a thermostatted, open chamber on an inverse microscope (Axiovert 135 TV, Carl Zeiss, Jena, Germany) equipped with a Plan-Neofluar 40×/0.75 lens (Carl Zeiss). Images were recorded with a standard CCD camera (C5403, Hamamatsu Photonics, Herrsching, Germany) and stored on videotape using a SVHS recorder (Panasonic AG-7350, Panasonic, Matsushita Electric Industrial Corp., Osaka, Japan).

Assembly of the transducer

Red blood cells were donated by one of the authors (D. A. Simson) directly before the experiments using a finger prick. The cells were suspended in phosphate-buffered saline containing 5 mM phosphate and washed several times using the same buffer. Osmotic strength was adjusted to 135 mosmol using sodium chloride. The buffer contained 0.1% (w/v) bovine serum albumin. The pH was adjusted to 7.4. Cells were washed three times before the experiments. All substances were bought from Sigma Chemical Co. (St. Louis, MO) and were of ACS quality. We used paramagnetic polystyrene latex beads with a diameter of 2.8 μm (Dynabeads M-280, Dynal, Oslo, Norway). The beads had reactive tosyl groups at the surface and were coated with wheat germ agglutinin (Sigma) according to the procedure given by the supplier of the beads. The coated beads were suspended in the same buffer as the red blood cells, stored at 4°C, and used within 3 days after preparation. Red blood cells and microbeads were mixed and injected into a small, open chamber on the microscope. Only swollen red blood cells that exhibited no or a tiny dimple were selected and aspirated with the micropipet. The beads were attached to the red blood cells by simply touching. In fortunate cases, a suitable red blood cell carried a microbead already. These preformed transducers were only rotated into the correct position. Temperature was kept constant at 18°C to prevent evaporation.

Magnetic tweezers

The basic setup of magnetic tweezers was described before (Ziemann et al., 1994). To achieve forces up to 1 nN we used an electromagnet with a chisel-shaped core of soft iron. The pointed end of this core protruded directly into the sample chamber. It was coated with a thin layer of nail varnish to prevent corrosion. A schematic view of the setup is displayed in Fig. 2. The electromagnet had 1200 turns, and currents up to 2.5 A were used. To calibrate the magnetic forces the sample chamber was filled with dimethylpolysiloxane (DMPS-1M, Sigma) exhibiting a viscosity of 976 mPa. Paramagnetic beads were suspended in dimethylpolysiloxane and positioned with the micropipet at distances of ~110 μm to the pointed end of the magnetic core. After switching on the electric current the beads started to move. The acting force was determined using Stokes' law. The forces were measured with at least ten different currents at one position. The magnetic force was found to depend linearly on current and increased with decreasing distance. Straight lines were fitted to the data using the least squares fit algorithm implemented in the data manipulation program Igor (Wavemetrics, Lake Oswego, OR). The so determined parameters were used to calculate the acting forces in the experiments. In the actual experiments the transducers were placed at a distance from 100 to 33 μm from the pointed end of the magnetic core and the force was applied as a triangular wave with a frequency of 0.5 Hz and force amplitudes from 40 to 500 pN. Identical results were obtained at frequencies of 50 mHz and 1 Hz.

Image processing

Image processing was done off-line using a Macintosh PowerPC 9500/200 (Apple Computer, Cupertino, CA) equipped with a frame grabber card (LG-3, Scion Corp., Frederick, MD). Images were digitized at video rate using the public domain image processing program NIH Image, version 1.60. The bead's image showed a central bright spot that was exploited for the measurement of the bead position. These were determined by nonlinear least squares fitting of the intensity profiles of the central bright spot using two-dimensional Gaussian functions. Displacements of the beads could be measured with an accuracy of at least 5 nm. This value was determined by embedding beads in two-component adhesive (Uhu Endfest 300, Uhu, Bühl, Germany). The positions of these beads were determined as described and showed a standard deviation of 4 nm in the x direction and 1 nm in the y direction at the highest magnification. In all measurements of force displacement relations the bead was moved in the x direction. In the measurements of the thermally driven motions, the axis of the transducer was aligned along the y direction of the camera.

Measurement of the force displacement relations

To determine the force displacement curves, bead positions of 5–10 consecutive cycles of the force were averaged. Raw and averaged data coincided within a few nanometers. Forces were calculated using the straight-line fits from the calibration procedure described in the magnetic tweezers section above. The same transducers were measured at different suction pressures. At low forces, the measured curves showed distortions that can be explained as follows. Most often the paramagnetic bead did not point exactly toward the pointed end of the magnetic core. Therefore, the magnetic force moved the bead slightly out of focus during the initial phase of a force cycle. Our algorithm for the determination of the bead position tracks the central bright spot of the bead's image. The position of this central spot on the bead was found to shift slightly with changing focus. This shift is unavoidable because the bead acts as a micro-lens. It is partially contrast matched to the buffer by the adhering red blood cell and thus creates an asymmetric, defocused image of the light source as a central bright spot. Therefore, motions perpendicular to the plane of focus couple

partially in the determined coordinate along the axis of the transducer. For this reason, the position of the bead at zero force had to be determined using linear extrapolation of the low-force part of the force displacement relations to zero force. Zero positions extrapolated at different suction pressures, and the measured zero position agreed, all within at most 100 nm.

Measurement of thermally driven vibrations

Thermally driven motions were determined in a separate series of experiments without the electromagnet present. The position of the bead was determined as before. Standard deviations of the bead position were calculated using at least 200 subsequent video frames. Suction pressures ranging from 30 Pa to 1000 Pa were used. This corresponds to membrane tensions from 20 μN/m to 700 μN/m.

RESULTS

Measured force displacement relations

Sixteen force displacement relations were determined using six different red blood cells. Force amplitudes ranged from 40 to 500 pN. In all cases, very good agreement between experimental results and numerically calculated curves was found. Some representative results are shown in Fig. 5. For extensions of more than 0.5 μm, nonlinearity is clearly apparent (see Fig. 6) as was expected from the calculations (see Fig. 4). Therefore, the theoretical description of the force transducer is adequate in this regime of forces. The distortions of the curves at very low forces were explained above in Materials and Methods.

Thermally driven vibrations

Observation of thermally driven bead motion enabled us to determine the transducer stiffness at the smallest elongations. The mean square amplitude $\langle x^2 \rangle$ is related to temperature by the equipartition theorem

$$\langle x^2 \rangle = \frac{k_B T}{k} \tag{27}$$

where $k_B T$ is the thermal energy and k denotes the transducer stiffness at small elongations, as given by Eqs. 25 and 26. Experimentally determined values for the fluctuations along the axis of the transducer are plotted in Fig. 7 versus the theoretical expected values. It is apparent that the determined values agree only in a very limited range with the theoretical expectation. For very stiff transducers we find a plateau value of $\sqrt{\langle x^2 \rangle}$. The plateau value was in this case 5 nm. If the bead is held directly in the pipet the root mean square amplitude is between 1 and 2 nm. The position of a bead held in the pipet can be determined with much higher accuracy than the position of a bead attached to a red blood cell. This is caused by fluctuations of the bead position perpendicular to the axis of symmetry that are opposed by the shear stiffness of the membrane only and are therefore of substantial amplitude (see Fig. 7). As explained above in Materials and Methods, motions of the bead perpendicular to the plane of focus result in erroneous changes of the determined coordinate of the bead along the axis of the transducer. For beads held directly in the pipet, perpendicular fluctuations are very small, and therefore this coupling of perpendicular motions is negligible.

For very low tensions, the amplitude of the thermally driven oscillation saturates. This happens at membrane tensions of roughly 20–30 μN/m. As the module for in-plane shear of the red blood cell membrane has been determined to be 10 μN/m (Evans, 1973; Hochmuth et al., 1973), we suppose that this leveling off at low membrane tensions happens because shear stress is no longer negligible and our theory breaks down. We want to point out that, using

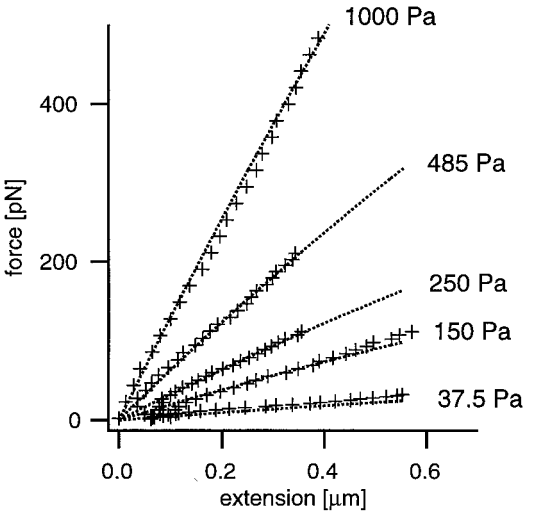

FIGURE 5 Force displacement relations for different suction pressures, indicated at the individual curves. Crosses represent measured values, and dotted lines represent calculated results. Parameters were as follows: $R_{0,0} = 3.5$ μm, $R_P = 0.95$ μm, and $R_a = 0.6$ μm.

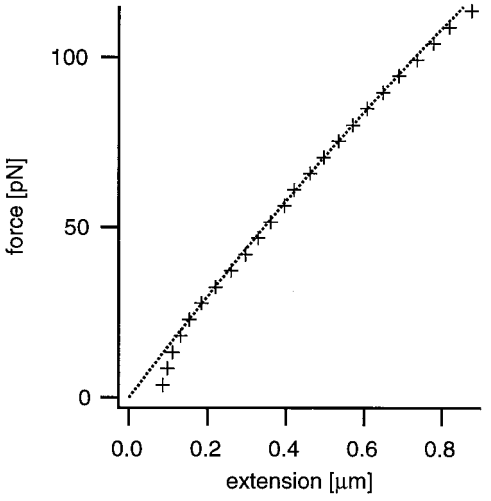

FIGURE 6 Force displacement relation for relatively large extensions. Crosses represent measured values; dotted lines represent calculated results. The geometrical parameters are given in Fig. 5, and suction pressure was 126 Pa.

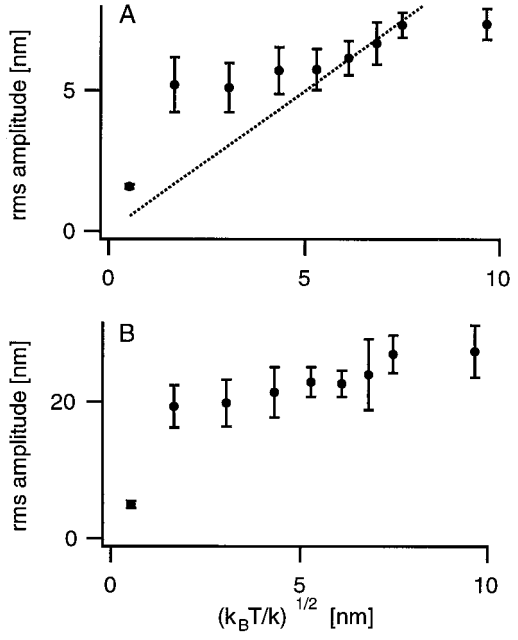

FIGURE 7 Thermally driven root mean square oscillations of the microbead along the axis of symmetry (*A*) and perpendicular to it (*B*). Please note the different scales. The dotted line represents the equipartition theorem for axial motions, Eq. 27. The first point of both curves represents the root mean square motions of a microbead held directly in a micropipet.

magnetic tweezers, we found good coincidence of theory and experiment even at a membrane tension of 25 μN/m. Taken together, this shows that the force transducer can be safely used only at membrane tensions exceeding 20 μN/m, corresponding to a stiffness at small elongations of approximately 45 μN/m.

The transverse stiffness of the transducer can be estimated from the equipartition theorem and the measured mean square amplitude of the perpendicular fluctuations to be approximately 10 μN/m.

DISCUSSION

The above described results clearly show that the micropipet-based force transducer is adequately described by our theory. Transducer stiffnesses, k, ranging from 45 μN/m to 10 mN/m can be selected. Bead positions can be determined to an accuracy of approximately 5 nm. Therefore, forces from 0.25 pN to 10 nN can be measured. Please note that the red blood cell could be replaced by a phospholipid vesicle. In that case, even lower stiffnesses and thus measurements of lower forces would be possible, because the in-plane shear module of a phospholipid membrane in the fluid phase is zero. Nevertheless, vesicles are in general very fragile. Moreover, an attached microbead will always sink under the influence of gravitation to the lowest position on the vesicle surface. For these reasons we preferred to use red blood cells.

Our theoretical analysis relies on the fact that the area of contact between the microbead and the red blood cell membrane remains unchanged under the influence of the applied external forces. Only the binding molecules in a very narrow zone along the rim of the contact zone are under tension (Evans, 1995). In our situation the tensile force acting on the adhesive molecules in this zone is proportional to $f/2\pi R_a$. If the bead membrane adhesion fails, R_a decreases and the bonds are exposed to even higher tensile stress. Therefore, the failure of the bead membrane adhesion is in this case a catastrophic event and not a gradual one. In all our experiments we never observed gradual peeling but only sudden failure of the microbead red blood cell adhesion.

The accuracy of this force measurement can be most easily analyzed in the case of small elongations using the approximate expression Eq. 26. As the full force displacement relations are only moderately nonlinear the relative error should be approximately the same in the full range of extensions studied here. We used Gaussian propagation of errors. In Table 1, the contributions of the different parameters to the final error are shown for a typical case. For these parameters the transducer stiffness at small elongations is 140 μN/m. The radius of the adhesion zone carries by far the largest error (30%), yet it contributes only moderately to the overall error. In contrast to this, the radius of the pipet has to be determined with very high accuracy (50 nm) to keep the overall error reasonable. For the parameters chosen here, a 10-pN force would lead to a transducer extension of 70 nm, which in turn could be measured with approximately 5 nm resolution. Therefore, a 10-pN force could be measured with an overall error of roughly 15%. Thus, the force transducer described here allows determination of very small forces with astonishing accuracy.

CONCLUSIONS

Recently, a very versatile, micropipet-based transducer for piconewton forces was introduced (Evans et al., 1995). The major advantage of this technique is the fact that the transducer stiffness can be easily tuned in the range from 45 μN/m to 10 mN/m during an experiment. In this paper we developed a method for the calculation of the force elongation relation of this force transducer. The results were verified by application of magnetic forces and by observation of thermal fluctuations. The range of accessible forces was explored. Forces in the range from 0.25 pN to 10 nN can be measured by this technique. We showed that such small

TABLE 1 Error contributions to the transducer stiffness *k*

Parameter	Value	Estimated error of the parameter	Contribution to the resulting error (%)*
R_0	3.0 μm	0.15 μm	5.2
R_a	0.5 μm	0.15 μm	9.3
R_p	1.0 μm	0.05 μm	8.6
ΔP	100 Pa	1 Pa	1.0
Total			14

*Contributions to the final error were calculated using Gaussian error propagation in Eq. 26.

forces can be measured with astonishing accuracy (approximately 15% for a 10-pN force). Thus it appears that this transducer is ideally suited for many applications that involve measurements of piconewton forces on microscopic length scales. Examples are the breaking of specific bonds and testing mechanical material properties at micron length scales.

We thank Erich Sackmann for generous support and encouraging discussions. One of the authors (R. Merkel) is indebted to Evan Evans for introducing him to this field of research. We are grateful to K. Andres and G. Görbel for the preparation of the SEM micrographs.

This work was supported by the Deutsche Forschungsgemeinschaft via the Sonderforschungsbereich 266.

REFERENCES

Alon, R., D. A. Hammer, and T. A. Springer. 1995. Lifetime of the P-selectin-carbohydrate bond and its response to tensile force in hydrodynamic flow. *Nature.* 374:539–542.

Ashkin, A., K. Schütze, J. M. Dziedzic, U. Euteneuer, and M. Schliwa. 1990. Force generation of organelle transport measured in vivo by an infrared laser trap. *Nature.* 248:346–350.

Bongrand, P., P. M. Claesson, and A. S. G. Curtis, editors. 1994. Studying Cell Adhesion. Springer, Berlin.

Chesla, S. E., and C. Zhu. 1996. Validation and accuracy assessment of the micropipet piconewton force transducer. *In* Advances in Bioengineering, BED, Vol. 33. S. Rastegar, editor. American Society of Mechanical Engineers, New York. 57–58.

Dammer, U., M. Hegner, D. Anselmetti, P. Wagner, M. Dreier, W. Huber, and H.-J. Güntherodt. 1996. Specific antigen/antibody interactions measured by force microscopy. *Biophys. J.* 70:2437–2441.

Discher, D. E., and N. Mohandas. 1996. Kinematics of red cell aspiration by fluorescence-imaged microdeformation. *Biophys. J.* 71:1680–1694.

Evans, E. A. 1973. New membrane concept applied to the analysis of fluid shear- and micropipette-deformed red blood cells. *Biophys. J.* 13: 941–954.

Evans, E. A. 1980. Analysis of adhesion of large vesicles to surfaces. *Biophys. J.* 31:425–431.

Evans, E. A. 1989. Structure and deformation properties of red blood cells: concepts and quantitative methods. *Methods Enzymol.* 173:3–35.

Evans, E. 1995. Physical actions in biological adhesion. *In* Structure and Dynamics of Membranes: Generic and Specific Interactions. R. Lipowsky and E. Sackmann, editors. North Holland, Amsterdam. 723–754.

Evans, E., D. Berk, and A. Leung. 1991. Detachment of agglutinin-bonded red blood cells. I. Forces to rupture molecular-point attachments. *Biophys. J.* 59:838–848.

Evans, E., and W. Rawicz. 1990. Entropy-driven tension and bending elasticity in condensed-fluid membranes. *Phys. Rev. Lett.* 64: 2094–2097.

Evans, E., K. Ritchie, and R. Merkel. 1995. Sensitive force technique to probe molecular adhesion and structural linkages at biological interfaces. *Biophys. J.* 68:2580–2587.

Evans, E., and R. Skalak. 1980. Mechanics and Thermodynamics of Biomembranes. CRC Press, Boca Raton, FL.

Evans, E. A., and R. Waugh. 1977. Osmotic correction to elastic area compressibility measurements on red cell membrane. *Biophys. J.* 20: 307–313.

Evans, E. A., R. Waugh, and L. Melnik. 1976. Elastic area compressibility modulus of red cell membrane. *Biophys. J.* 16:585–595.

Finer, J. T., R. M. Simmons, and J. A. Spudich. 1994. Single myosin molecule mechanics: piconewton forces and nanometre steps. *Nature.* 368:113–119.

Florin, E.-L., V. Moy, and H. E. Gaub. 1994. Adhesion forces between individual ligand-receptor pairs. *Science.* 264:415–417.

Gröbner, W., and N. Hofreiter. 1975. Integraltafeln. Erster Teil. Unbestimmte Integrale. Fünfte, verbesserte Auflage. Springer-Verlag, Wien.

Heinrich, V., and R. E. Waugh. 1996. A piconewton force transducer and its application to measurement of the bending stiffness of phospholipid membranes. *Ann. Biomed. Eng.* 24:559–605.

Hochmuth, R. M., N. Mohandas, and J. P. L. Blackshear. 1973. Measurement of the elastic modulus for red cell membrane using a fluid mechanical technique. *Biophys. J.* 13:747–762.

Hochmuth, R. M., J.-Y. Shao, J. Dai, and M. P. Sheetz. 1996. Deformation and flow of membrane into tethers extracted from neuronal growth cones. *Biophys. J.* 70:358–369.

Kishino, A., and T. Yanagida. 1988. Force measurements by micromanipulation of a single actin filament by glass needles. *Nature.* 334:74–76.

Kuo, S. C., and D. A. Lauffenburger. 1993. Relation between receptor/ligand binding affinity and adhesion strength. *Biophys. J.* 65:2191–2200.

Lee, G. U., D. A. Kidwell, and R. J. Colton. 1994. Sensing discrete streptavidin-biotin interactions with atomic force microscopy. *Langmuir.* 10: 354–357.

Needham, D. 1993. Measurement of interbilayer adhesion energies. *Methods Enzymol.* 220:111–129.

Pierres, A., A.-M. Benoliel, and P. Bongrand. 1995. Measuring the lifetime of bonds made between surface-linked molecules. *J. Biol. Chem.* 270: 26586–26592.

Shao, J.-Y., and R. M. Hochmuth. 1996. Micropipette suction for measuring piconewton forces of adhesion and tether formation from neutrophil membranes. *Biophys. J.* 71:2892–2901.

Simmons, R. 1996. Molecular motors: single-molecule mechanics. *Curr. Biol.* 6:392–394.

Stoer, J., and R. Bulirsch. 1993. Introduction to Numerical Analysis, 2nd ed. Springer-Verlag, New York.

Svoboda, K., C. F. Schmidt, B. J. Schnapp, and S. M. Block. 1993. Direct observation of kinesin stepping by optical trapping interferometry. *Nature.* 365:721–727.

Tees, D. F. J., and H. L. Goldsmith. 1996. Kinetics and locus of failure of receptor-ligand-mediated adhesion between latex spheres. I. Protein-carbohydrate bond. *Biophys. J.* 71:1102–1114.

Yeung, A. K. C. 1994. Mechanics of inter-monolayer coupling in fluid surfactant bilayers. Ph.D. thesis, University of British Columbia.

Zhu, C., T. E. Williams, J. Delobel, D. Xia, and M. K. Offermann. 1994. A cell-cell adhesion model for the analysis of micropipette experiments. *In* Cell Mechanics and Cellular Engineering. V. C. Mow, F. Guilak, R. Tran-Son-Tay, and R. M. Hochmuth, editors. Springer Verlag, New York. 160–181.

Ziemann, F., J. Rädler, and E. Sackmann. 1994. Local measurements of viscoelastic moduli of entangled actin networks using an oscillating magnetic bead micro-rheometer. *Biophys. J.* 66:2210–2216.

Zilker, A., M. Ziegler, and E. Sackmann. 1992. Spectral analysis of erythrocyte flickering in the 0.3–4 μm^{-1} regime by microinterferometry combined with fast image processing. *Phys. Rev. A.* 46:7998–8001.